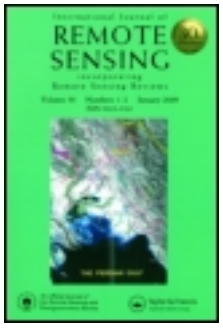

International Journal of Remote Sensing

Publication details, including instructions for authors and subscription information:
http://www.tandfonline.com/loi/tres20

Investigation of polynya dynamics in the northern Bering Sea using greyscale morphology image-processing techniques

Hongli Fu [a], Jinping Zhao [a] & Karen E. Frey [b]

[a] College of Physical and Environmental Oceanography, Ocean University of China, Qingdao, Shandong, 266100, PR China

[b] Graduate School of Geography, Clark University, Worcester, MA, 01610, USA

Available online: 19 Sep 2011

To cite this article: Hongli Fu, Jinping Zhao & Karen E. Frey (2011): Investigation of polynya dynamics in the northern Bering Sea using greyscale morphology image-processing techniques, International Journal of Remote Sensing, DOI:10.1080/01431161.2011.608088

To link to this article: http://dx.doi.org/10.1080/01431161.2011.608088

International Journal of Remote Sensing
iFirst, 2011, 1–19

Investigation of polynya dynamics in the northern Bering Sea using greyscale morphology image-processing techniques

HONGLI FU*†, JINPING ZHAO† and KAREN E. FREY‡
†College of Physical and Environmental Oceanography, Ocean University of China, Qingdao, Shandong 266100, PR China
‡Graduate School of Geography, Clark University, Worcester, MA 01610, USA

(*Received 6 February 2010; in final form 17 May 2011*)

Arctic coastal polynyas, defined here as persistent openings in the winter sea ice pack, are significant areas for ocean–atmosphere heat exchange, high winter sea ice production with resulting brine rejection and the dependence of local ecosystems. It is therefore critical to accurately quantify polynya dynamics to understand their spatial and temporal variability, particularly in the context of recent dramatic Arctic sea ice declines. In this study, the so-called erosion algorithm (a greyscale morphology image-processing technique) is applied to satellite-derived sea ice concentrations in the northern Bering Sea to investigate polynya dynamics throughout this region. Greyscale morphology allows for the estimation of sea ice extent with a defined error tolerance through the removal of regions with low sea ice concentrations in the marginal ice zone. Furthermore, since polynyas are the primary source of water within the sea ice pack, the presence of water here can therefore be utilized to define the areal extent of polynyas. We utilized AMSR-E (Advanced Microwave Scanning Radiometer-EOS) sea ice concentrations during January–April from 2003 to 2008 in the northern Bering Sea to extract daily time series of water area within polynyas by a water integration method after data are preprocessed using greyscale morphology techniques. These results compare well with those calculated by more traditional methods utilizing sea ice concentration thresholds and show the great utility of greyscale morphology techniques as a preprocessing method (which eliminates artificial determination of polynya areal extents and enables automation of the overall image-processing routine). In addition, based on the results of our algorithms we investigated the potential driving forces (e.g. offshore wind velocity) of polynya development in the northern Bering Sea as well as calculate the spatial and interannual variability of heat fluxes across these water surfaces owing to polynya formation.

1. Introduction

Polynyas are defined as either partially or totally ice-free areas in an otherwise ice-covered region, whose area and location are variable with atmospheric conditions (World Meteorological Organization (WMO) 1970). According to the mechanism by which they are formed and/or maintained, polynyas are traditionally categorized into two classes: 'sensible heat' and 'latent heat' polynyas (Smith *et al.* 1990, Maqueda *et al.* 2004). Latent heat polynyas are mechanically driven in areas where

*Corresponding author. Email: fhlkjj@163.com

International Journal of Remote Sensing
ISSN 0143-1161 print/ISSN 1366-5901 online © 2011 Taylor & Francis
http://www.tandf.co.uk/journals
http://dx.doi.org/10.1080/01431161.2011.608088

the ice motion is divergent because of prevailing winds or oceanic currents. Because locally formed ice is advected downstream and the heat of the water is released into the atmosphere, the water within the polynya (which is typically near the freezing point) is continually converted into ice. Sensible heat polynyas appear as a result of oceanic sensible heat entering the area of polynya formation in amounts large enough to melt any pre-existing ice and prevent the growth of new ice. Sensible heat polynyas are therefore typically areas of low ice production, and their sizes are determined by the dimensions of the warm water influences. Latent and sensible heat polynyas are not necessarily mutually exclusive, but in many cases are coexistent.

Polynyas play a critical role in local and regional climate variability. First, polynya regions are significant sources of moisture and heat from the ocean to the atmosphere. In winter, approximately 50% of the total ocean–atmosphere heat exchange over the Arctic Ocean occurs through polynyas and leads (Maykut 1982). During summer, polynyas allow large quantities of short-wave radiation to penetrate the oceanic mixed layer, which ultimately impacts ocean warming and sea ice pack mass balance (Maykut and Perovich 1987, Maykut and McPhee 1995). Second, brine rejection during the formation of frazil ice within polynya areas increases the salinity of the upper ocean. The so-called Arctic halocline is likely maintained by the advection of cold saline water formed as a result of sea ice growth over the continental shelves of the Arctic Ocean and the Bering Sea (Aagaard *et al.* 1981, Cavalieri and Martin 1994, Winsor and Bjork 2000). Because of brine rejection and buoyancy loss upon sea ice formation, cold and saline dense water is produced within coastal polynyas, which then flows downslope to the deeper ocean basin. This is an important mechanism of ventilating deep and bottom water in both the Southern Ocean and the Arctic Ocean (Grumbine 1991, Emms 1997, Comiso and Gordon 1998). Third, polynyas are likely sites of relatively high primary and secondary productivity (Grebmeier and Cooper 1995, Stirling 1997). Thus, polynya waters are ultimately important habitats for migratory waterfowl and marine mammals. Continuous and accurate monitoring of the location and extent of polynya regions is therefore critical to the study of the climate system and energy exchange, physical oceanography and ocean circulation, and biological and ecosystem components of the Arctic.

Winter ice formation in the northern Bering Sea has been described with a 'conveyor belt' analogy (Niebauer *et al.* 1999). Polynyas primarily occur in regions with the coasts at the northern end, as the predominantly northerly wind drives sea ice southwards away from the coasts (McNutt 1981). Major polynya systems in the Bering Sea occur southwards or downwind of the Chukchi Peninsula, St Lawrence Island and the Seward Peninsula (Niebauer *et al.* 1999). Polynyas may also occur along the coasts in the southern regions of the northern Bering Sea under southerly wind conditions, although this is rare during winter (Stringer and Groves 1991).

Polynyas are widely distributed across most of the polar region and are highly variable, both spatially and temporally. While field observations of polynyas have been quite limited, satellite sensors provide much needed observational time series of polynya dynamics. Based on the Advanced Very High Resolution Radiometer (AVHRR) visible satellite images, Stringer and Groves (1991) analysed polynyas in the Bering Sea and Chukchi Shelf, obtaining high spatial resolution areal extents of polynya regions. However, observations utilizing visible and near-infrared satellite imagery are severely limited by the presence of fog and clouds as well as by the absence of sunlight during winter periods.

Microwave sensors enable all-weather monitoring of polynyas, even during polar night conditions (Markus and Burns 1995). Various products of microwave remote sensing (e.g. sea ice concentration) can be used to observe polynya variability. Sea ice is discontinuous within polynya regions, whereas satellite images of sea ice are typically processed as a continuous medium with variable concentrations. Algorithms are therefore necessary to convert sea ice concentrations to polynya regions. At present, there are two methods to depict polynyas from sea ice concentration data. One method is based on a specified sea ice concentration threshold (hereafter referred to as the threshold method). If pixels with values lower than the specified threshold are surrounded by values higher than the specified threshold, they are considered to be polynya areas. Massom *et al.* (1998) analysed latent heat polynyas in the Southern Ocean with an ice concentration threshold of 0.75. Using AMSR-E (Advanced Microwave Scanning Radiometer-EOS) ice concentration data, Parmiggiani (2006) also used a 0.75 threshold. Smedsrud *et al.* (2006) simulated the Storfjorden polynya through a high-resolution ocean–sea ice-coupled model and found that the ice concentrations at the edge of polynyas were typically distributed between 0.60 and 0.70. Moreover, sea ice concentrations in the marginal zone of polynyas will be influenced by the parameters of microwave sensors, the retrieval algorithms for ice concentrations and the spatial and temporal variability of polynya formation. By comparing different reversion methods of AMSR-E ice concentrations, Kwok *et al.* (2007) noticed that the ice concentration obtained by the ABA (AMSR-E Bootstrap) retrieval algorithm was 0.83, while that obtained by the NT2 (NASA Team 2) retrieval algorithm was 0.91 on the same edge of ice. Kern *et al.* (2007) studied a variety of polynyas through multiple algorithms and found that ice concentration thresholds range between 0.05 and 0.40 in regions of water and between 0.65 and 0.80 in regions of thin ice. Since ice concentrations may indicate continuous shifts from pack ice to open water (and a distinct border does not necessarily exist between pack ice and polynyas), the selection of thresholds inherently affects the size of the polynya areas.

An additional method of polynya detection is based on the simple area integration of the water within a polynya (rather than utilizing a sea ice concentration threshold > 0). This method is hereafter referred to as the water integration method. Because water area in a polynya is proportional to the overall size of this polynya, this parameter can also be utilized to estimate total polynya area (e.g. Cavalieri and Martin 1994). The advantage of the water integration method is that it avoids the arbitrary selection of a threshold, while still quantifying the net water area in the polynya. Since low ice concentrations can depict not only polynyas but also marginal ice zones of the overall sea ice pack, this method requires an artificial determination of the polynya extent. The key to this approach is how to eliminate the marginal ice zone from the process to calculate only the water area within a given polynya. The result of the water integration method is therefore relatively subjective and the lack of the ability to automate this process is inconvenient (particularly when long image time series are investigated). Therefore, the water integration method has thus far not been extensively utilized.

In this study, a new erosion algorithm based on greyscale morphology is proposed to accurately quantify the water area of polynyas or leads from satellite-derived sea ice concentrations. This new algorithm eliminates low sea ice concentrations in the marginal ice zone of the overall sea ice pack to avoid the disadvantage of the simple water integration method. This new algorithm also provides an approach to analyse and automate the process for a large number of images necessary to investigate the temporal nature of polynya dynamics. The erosion algorithm is applied to the AMSR-E daily ice concentrations during January–April of 2003–2008 to compute the

daily water areas within the extent of all polynyas in the northern Bering Sea. The results are compared with that obtained by the more traditional sea ice concentration threshold method. Interseasonal and interannual variability of the polynya water areas and the resulting heat fluxes are presented. Potential drivers of polynya size are also investigated by correlating the coefficient between polynya water area and offshore wind speed.

2. Data and methods

2.1 *Data*

The daily sea ice concentration data are derived from AMSR-E radiance values using the NT2 algorithm with a spatial resolution of 12.5 km and temporal extent from 19 June 2002 to 31 May 2008. These data can be accessed from the website of the National Snow and Ice Data Center (NSIDC) (http://nsidc.org/data/ae_si12.html). Daily meteorological data extracted from the National Centers for Environmental Prediction (NCEP) reanalysis data from 2003 to 2008 are used to calculate a variety of heat fluxes through the water surface. The reanalysis data are on a T62 Gaussian grid with a resolution of 2.5°. The meteorological data include parameters of 10 m wind, surface air temperature, surface specific humidity, surface downward solar radiation flux and surface downward long-wave radiation flux.

The Bering Sea map is plotted using a Lambert azimuthal equal-area projection (see figure 1). The origin of the coordinate is chosen at the North Pole (90° N) and

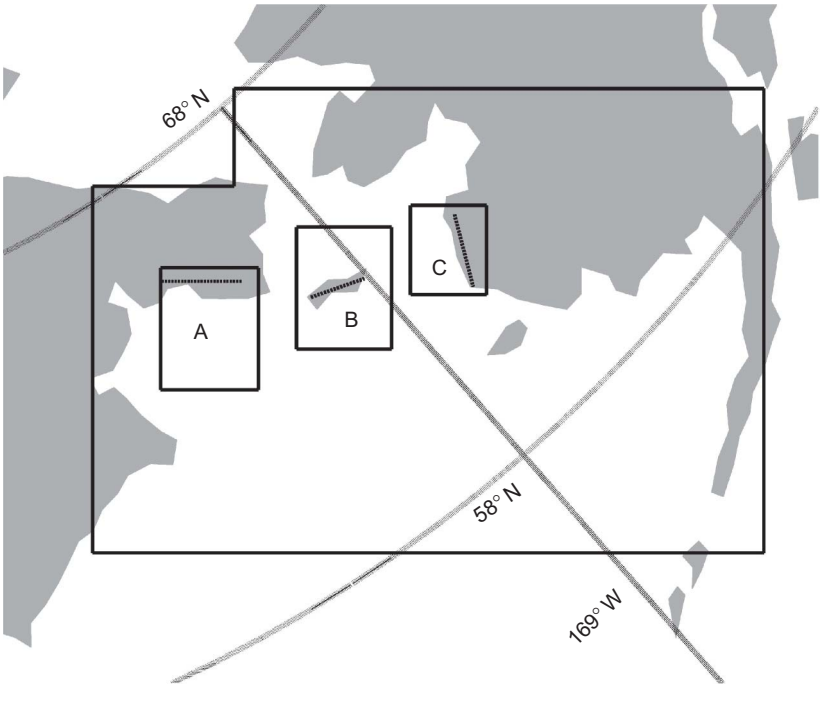

Figure 1. The black frame indicates the study area in the Bering Sea. The boxes A, B and C present the main area of the Anadyr Gulf polynya, the St Lawrence Island polynya and the Cape Romanzo polynya, respectively. The dashed lines in the boxes A, B and C indicate the general orientations of the coastlines.

the *y*-axis is along 150° E. The black frame in figure 1 indicates the study area, which includes 252 × 191 grid cells with a 6.37 km pixel spacing. The full time series of ice concentration data are interpolated to these grid cells by linear interpolation to calculate the water area of existing polynyas and their associated surface heat fluxes.

2.2 *Water integration method*

In an ice-covered region S, a certain proportion of water exists if the ice concentration at some grid cells is less than 1. The water area in this region, S_w, can be calculated by

$$S_w = \int_S (1 - C_i) dS_i, \tag{1}$$

where C_i is the ice concentration of the ith cell and dS_i is the area of the ith grid cell. S_w includes the water area within polynyas, leads and the marginal ice zone. If the water in the marginal ice zone is effectively removed, as is the goal with this water integration method, S_w will only include the water area in polynyas and leads (which are the most important parameters for determining the inner open water area of polynyas).

2.3 *Erosion algorithm*

Ice-covered areas are typically composed of polynyas, leads, pack ice, as well as the marginal ice zone. In many cases, these zones are interleaved and difficult to distinguish from one another. To calculate the net water area in polynyas and leads by the water integration method, the marginal ice zone must first be identified and removed to ensure the accuracy of the calculated overall water areas. As the waters in the marginal ice zone and in polynyas are similar and cannot be separated using ice concentration values alone, a method to eliminate the marginal ice zone based only on concentrations must be determined. The erosion algorithm of greyscale morphology presented here is indeed a method that allows one to identify and separate the water areas in marginal ice zones from those in polynyas and leads.

Morphology describes a broad set of image-processing operations. Utilizing morphological operations, a structuring element is applied to an input image to create an output image with an identical spatial extent. All morphological operations are based on two fundamental operations: erosion and dilation. Erosion is a method applied to eliminate pixels from the margin through to the interior of an image. By repeating the erosion operation, the surrounding marginal ice zone pixels can be systematically eliminated and the water in a marginal ice zone eventually converges to open water. If the pixels removed encounter pack ice, the erosion process halts at these pixels and then continues towards other pixels until all marginal ice zone pixels ultimately encounter pack ice. A reasonable criterion for pack ice is chosen by its concentration, as a high value of concentration will distinguish pack ice from the marginal ice zone and polynyas. Eventually, the marginal ice zone is removed (or 'eroded') and the polynyas remain in the output image.

If $f(x,y)$ denotes the input image and $g(x,y)$ denotes the structuring element, the erosion result $(f \Theta g)(s,t)$ of $f(x,y)$ by $g(x,y)$ is expressed as follows (Dougherty 1993):

$$(f \Theta g)(s,t) = \min \{ f(x,y) | (x,y) \in D[g(x-s, y-t)] \}, \tag{2}$$

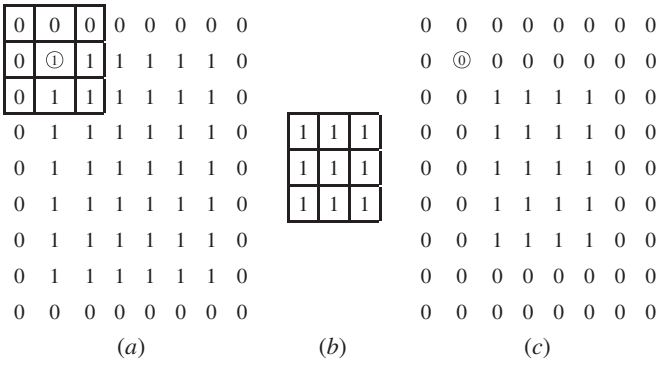

Figure 2. (*a*) The 9 × 8 matrix **f**, (*b*) the 3 × 3 square structuring element $\mathbf{g}_0$ and (*c*) the erosion result of **f** by $\mathbf{g}_0$ ($\mathbf{f}\Theta\mathbf{g}_0$).

where $g(x–s,y–t)$ is the translation of $g(x,y)$ (by which its centre pixel is translated to the pixel to be processed at (s,t)), $D[g(x–s,y–t)]$ represents the coordinates for the neighbourhood pixels surrounding (s,t) and Θ denotes the sign of the erosion operation in the greyscale morphology image processing technique. Choosing a 3 × 3 matrix $\mathbf{g}_0$ with each pixel value being 1 as the structure element (see figure 2(*b*)) and applying it to image **f** (a 9 × 8 matrix (see figure 2(*a*))), the neighbourhood includes the central pixel and the eight surrounding pixels (see figure 2(*a*)). Based on equation (2), the value of the circled pixel in the output image (see figure 2(*c*)) is the minimum value of the nine pixels of the neighbourhood (see figure 2(*a*)). If 0 denotes water and 1 denotes ice, the boundary of the ice-covered region in the original image **f** shrinks. The marginal ice zone can therefore be excluded from the pack ice cover by systematically utilizing the erosion operation.

2.4 *Sea ice extent*

The northern region of the Bering Sea freezes initially in November each year with the ice boundary extending gradually southwards over the subsequent weeks. The ice extent typically reaches its maximum in mid-March of the following year, covering nearly the entire continental shelf of the Bering Sea. A number of latent heat polynyas form along the south-facing coastlines throughout the region as a result of persistent northerly winds. Figure 3 indicates the daily ice concentrations in the Bering Sea on 2 March 2003. Only when the marginal ice zone is excluded from the pack ice domain can the water area be integrated through equation (1) to accurately represent the size of all polynyas or leads in the Bering Sea. Polynyas are a typically much more important source of open water than leads, and so the calculations of open water areas outside the marginal ice zone are primarily comprised by the presence of polynyas.

In order to calculate the sea ice extent throughout the region, we first need to calculate the ice-covered areas from the ice concentration field by eliminating the open water pixels. For water areas in the proximity of sea ice, we need to determine whether they connect with the open water areas south of the sea ice edge. If they link to large areas of open water, they are removed from the ice-covered area and marked by '0'. Otherwise, for the zero concentration grids in some isolated areas completely contained within the sea ice pack, they belong to the ice-covered area and are marked by '1'. The pink

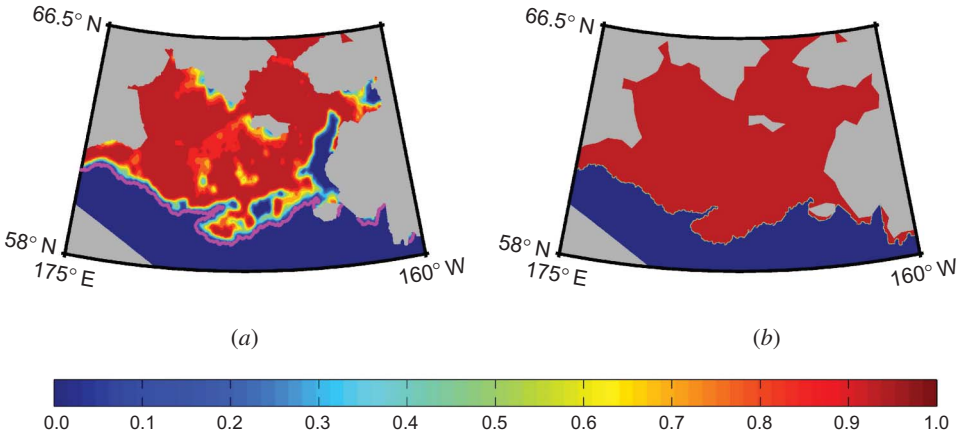

Figure 3. Fractional ice concentrations with (*a*) the marginal sea ice edge (pink line) and (*b*) the extent of ice (red region) in the northern Bering Sea on 2 March 2003.

line in figure 3(*a*) is the edge of ice obtained through the above method and the red domain in figure 3(*b*) is the extent of the ice-covered area including polynyas as well as the marginal ice zone.

Second, the erosion algorithm is applied to eliminate the water pixels in the marginal ice zone. As mentioned in §2.3, the erosion algorithm (through the structuring element $\mathbf{g}_0$) allows for the elimination of water pixels in the marginal ice zone. If the erosion algorithm is operated repeatedly until the marginal ice zone is entirely eliminated, the water remaining within the ice-covered regions can be attributed entirely to the presence of polynyas and/or leads. While the erosion algorithm is operated continuously, the elimination of water pixels will slow down when the ice concentrations of the pixels removed in the region become higher. If the water area is nearly unchanged during this process, the eroding process could stop, and the water area is equal to the total water area of all polynyas and/or leads. The relative error of the erosion process is defined as the change of the water area between two erosion steps divided by the total water area in the original ice area. When this relative error becomes negligible, the erosion process is stopped. In this study, we empirically determined that 0.01 is an acceptable relative error level. As such, our eroding process completes when the relative error is less than 0.01 and the water area is then quantitatively confirmed. When the erosion has reached the pack ice, further erosion is unnecessary. Therefore, another criterion is chosen when a gridded ice concentration is greater than 0.95. The eroding process will be interrupted at those grid cells, but continues through cells with less than 0.95 ice concentration. The total water area ultimately obtained from equation (1) is equal to the water area within all polynyas and/or leads of the entire Bering Sea region.

Figure 4 shows Bering Sea ice concentrations on 2 March 2003. There are a number of areas with low ice concentration within the total pack ice region (figure 4(*a*)). Using the erosion algorithm described above, the southern ice edge continuously shrinks as the grid cells of the marginal ice zone are gradually converted into open water when the erosion operation increases from 5 iterations (figure 4(*a*), green line) to 16 iterations (figure 4(*a*), blue line). As the calculated relative error drops below 0.01 after the 16th erosion iteration, the eroding process halts and the remaining ice is defined as pack ice. The remaining pack ice region (see figure 4(*b*)) is then used to calculate the

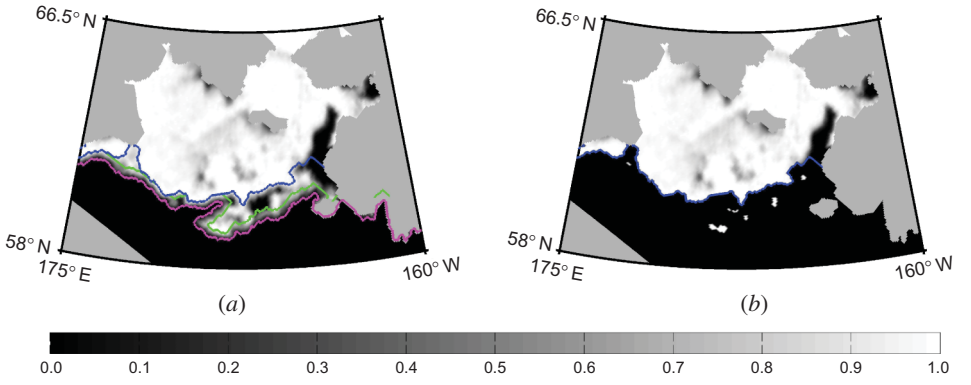

Figure 4. (*a*) Daily sea ice concentrations showing the marginal sea ice edge (pink line), sea ice edge after being eroded 5 times (green line) and sea ice edge after being eroded 16 times (blue line) on 2 March 2003. (*b*) Daily sea ice concentration within the extent of the pack ice on 2 March 2003.

water area for polynyas and leads by the water integration method using equation (1), which are the only water areas remaining now that the marginal ice zone water areas have been removed. Figure 4 suggests that the extent of the pack ice obtained through the water integration method (with preprocessing through the erosion algorithm) is reliable and the polynya and/or lead water areas calculated are accurate (after the marginal ice zone water areas have been completely removed). The erosion algorithm presented here is thus a preprocessing method, which has great utility by both eliminating artificial determination of polynya areal extents and automating the overall image-processing routine. As a preprocessing technique, the erosion algorithm can be used by the water integration method, threshold method and/or other potential methods based on simple ice concentrations.

The erosion algorithm is a preprocessing method, which removes the marginal ice zone from pack ice and improves on other methods to solve polynya parameters as shown in figure 4. To validate the erosion method, we compared results of the erosion method for both a Moderate Resolution Imaging Spectroradiometer (MODIS) image of calibrated radiances (250 m resolution) and an AMSR-E sea ice concentrations. We show a portion of the marginal ice zone in the northern Bering Sea on 10 March 2008 as an example (figure 5), where (*a*) is the MODIS image and (*b*) is the AMSR-E image. The erosion algorithm was applied to the AMSR-E image shown in figure 5(*b*) to remove the marginal ice zone from the pack ice, with the final result plotted as the black line in both panels of figure 5. The removal of the marginal ice zone through the erosion algorithm is quite robust when applied to the AMSR-E image. This is indeed validated when applied to the high-resolution 250 m MODIS image (figure 5(*a*)). The erosion method can thus be a useful tool to remove the marginal ice zone using sea ice concentration data at a variety of spatial resolutions.

3. Results and discussion

3.1 *Polynya water areas*

Daily ice concentrations in the Bering Sea over the winter period January–April from 2003 to 2008 are analysed by the erosion algorithm based on greyscale morphology

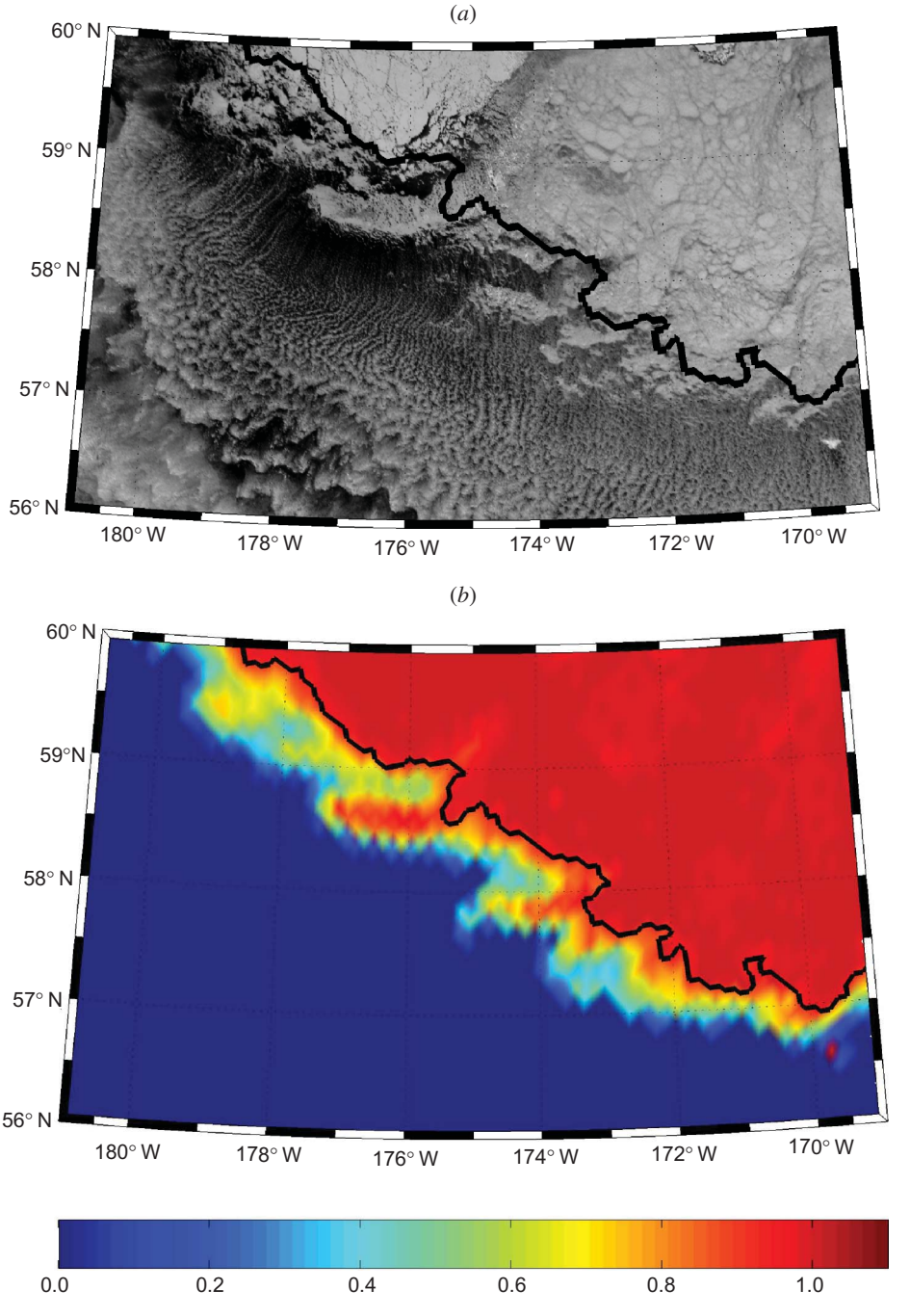

Figure 5. Comparison of erosion algorithm results for AMSR-E ice concentrations and high-resolution MODIS data on 10 March 2008. (*a*) MODIS image of calibrated radiance data (250 m resolution) and (*b*) AMSR-E image of sea ice concentration data. The black line in both panels is the final result after removing the marginal ice zone from pack ice using the erosion algorithm presented in this study.
Note: AMSR-E, Advanced Microwave Scanning Radiometer-EOS; MODIS, Moderate Resolution Imaging Spectroradiometer.

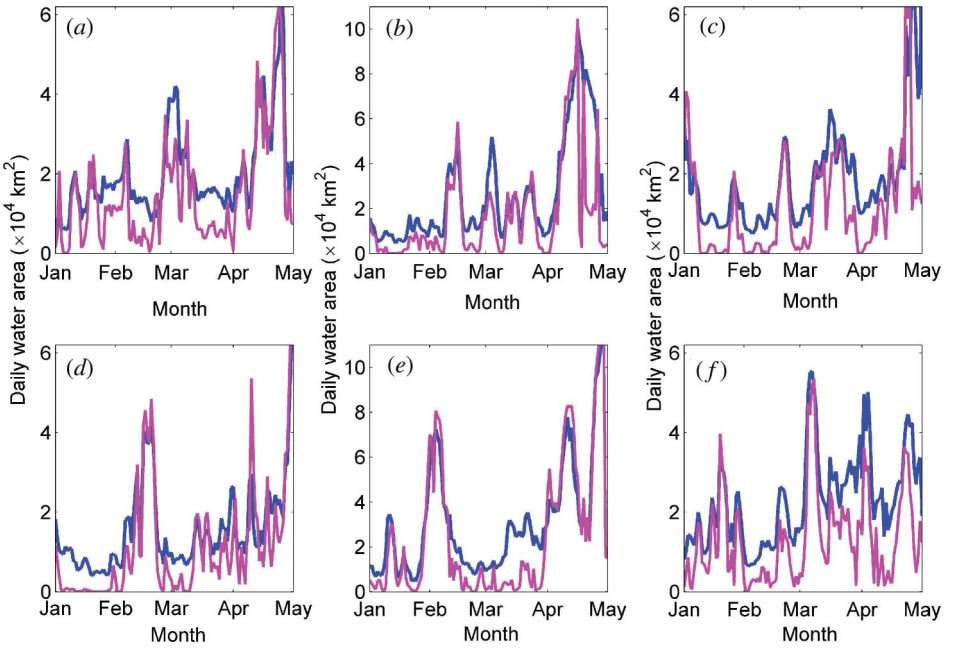

Figure 6. Daily water areas of all polynyas calculated according to the water integration method with erosion algorithm (blue line) and the ice concentration threshold method (pink line) during January–April of (*a*) 2003, (*b*) 2004, (*c*) 2005, (*d*) 2006, (*e*) 2007 and (*f*) 2008.

described in §2. Accordingly, the extent of pack ice for each day is obtained and the daily water area of all polynyas in the Bering Sea is calculated (figure 6, blue line). The annual peak of total water area shows that polynya areas have expanded significantly over our observed time series from January through April. With the ice concentration threshold method, the water area of all polynyas is the total area of pixels with values lower than the specified threshold in the pack ice, the extent of which must be delimited subjectively (Massom *et al.* 1998). Within a polynya and/or lead, the water integration method integrates only the water fractional area based on the ice concentration for each pixel, while the threshold method assumes a pixel to be entirely ice (water) if its concentration is greater (less) than the threshold (e.g. 0.75). Therefore, the area of a polynya calculated with the water integration method (after erosion) is the net water area with no sea ice included, while the area calculated with the threshold method includes up to 0.75 sea ice. Comparisons of the daily water areas by the water integration method using the erosion algorithm (figure 6, blue line) with those calculated by the ice concentration threshold method (figure 6, pink line) show visible differences. Pearson's correlation coefficients of the areas of polynyas obtained by the two methods over the years 2003–2008 are 0.87, 0.74, 0.64, 0.93, 0.81 and 0.87, respectively. An additional advantage of the erosion algorithm is that it provides a more reasonable physical representation of a mixed water/sea ice pixel within polynyas and leads, therefore providing a more accurate calculated water area within these regions. As such, the water integration method using the erosion algorithm for calculating water areas within a sea ice pack (only limited by the spatial resolution of the satellite data) is a superior method to directly estimate the ocean–atmosphere heat exchange through polynyas, potential brine production from polynya formation,

and the potential wintertime habitat of migratory waterfowl and marine mammals throughout the region.

3.2 *Monthly and interannual variability of polynya water areas*

Table 1 shows the monthly (January–April) water areas of all polynyas by the water integration method and erosion algorithm from 2003 to 2008, as well as the average January–April total period for each year. Generally, the maximum of the water area occurs in April, while the minimum in January. The water areas in February and March show little interannual variability (see figure 7). These observations are consistent with the seasonal variability of sea ice cover as a whole within the northern Bering Sea region. In January, few polynyas exist because most areas within the study area are still ice-free. After January, sea ice typically covers the entire continental shelf of the Bering Sea. As a result of consistent northerly offshore winds, most polynyas are open during February and March, leading to a gradual increase of the water areas

Table 1. Average of daily water areas (km^2) of all polynya areas.

Year	Jan	Feb	Mar	Apr	Jan–Apr
2003	13 670	17 872	19 019	29 905	20 092
2004	9 347	19 631	21 557	53 109	25 849
2005	12 862	11 241	21 056	28 702	18 561
2006	7 824	19 209	12 863	22 846	15 538
2007	16 217	27 893	22 348	62 480	32 091
2008	17 126	13 474	31 292	29 545	23 039

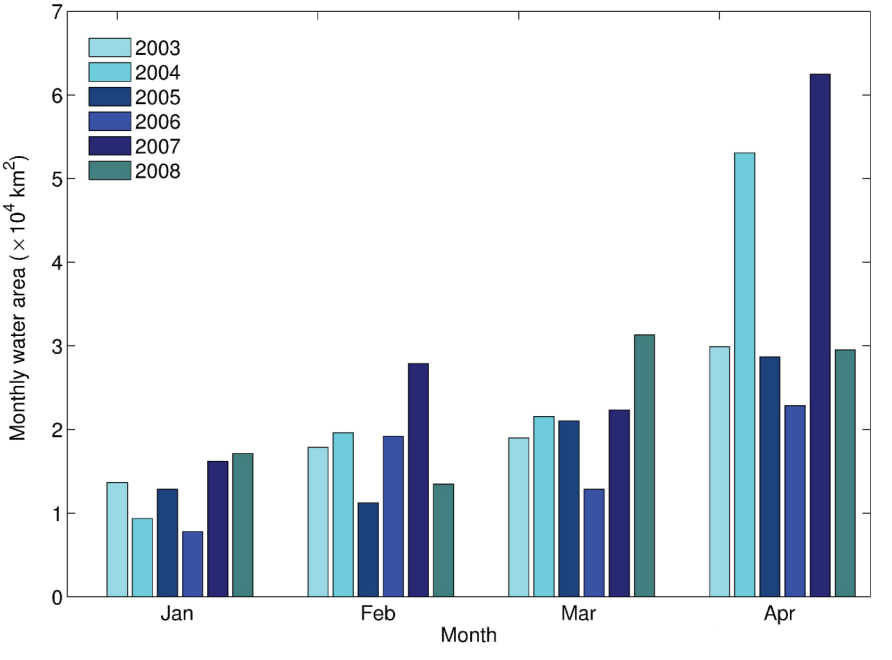

Figure 7. Monthly water areas for all polynyas during January–April of 2003–2008.

throughout the region during this time period. During April, stronger solar radiation is absorbed by polynya areas resulting in enhanced rates of sea ice melt and lowered albedo, which in turn speeds the melt process owing to ice-albedo positive feedbacks. Comparisons of monthly water areas across years (table 1 and figure 7) show that months during the year 2007 have consistently larger water areas than the same period in other years. These observed maximum areas of polynyas in the northern Bering Sea are consistent with the lowest record of the Arctic ice area in the summer of 2007 (Comiso *et al.* 2008).

3.3 *Heat exchange through polynya surface waters*

In this study, our heat flux calculations are based on the assumption that the water column temperatures within polynya areas are at the freezing point, T_0. In this case, any surface cooling will result in ice production. The net atmosphere-to-ocean heat flux, F_{net}, at the surface of polynya areas is given by

$$F_{\text{net}} = (1-\alpha)F_{\text{r}} + F_{\text{L}} - \varepsilon\sigma T_0^4 + F_{\text{s}} + F_{\text{e}}, \tag{3}$$

where α is the albedo; ε is the long-wave emissivity; $\sigma = 5.67\times10^{-8}$ W m^{-2} K^{-4} is the Stefan–Boltzmann constant; F_{r} is the incident short-wave radiation; F_{L} is the incoming long-wave radiation; $\varepsilon\sigma T_0^4$ is the upward long-wave radiation; F_{s} is the sensible heat flux; and F_{e} is the latent heat flux. The sensible heat flux was taken to be $F_{\text{s}} = \rho c_{\text{p}} C_{\text{s}} u(T_{\text{a}} - T_0)$, where T_{a} is the air temperature; $\rho = 1.3$ kg m^{-3} is the air density; $c_{\text{p}} = 1004$ J kg^{-1} K^{-1} is the specific heat of the air; C_{s} is the transfer coefficient for sensible heat; and u is the wind speed. The latent heat flux was taken to be $F_{\text{e}} = \rho L_{\text{v}} C_{\text{e}} u(q_{\text{a}} - q_0)$ (Haltiner and Martin 1957), where $L_{\text{v}} = 2.49 \times 10^6$ J kg^{-1} is the latent heat of vaporization of water; C_{e} is the transfer coefficient for latent heat; q_{a} is the humidity of the air; and q_0 is the humidity of the surface. The value q_0 was calculated as $q_0 = 0.622e/(P_0 - 0.37e)$ (Hess 1959), where $P_0 = 1.013 \times 10^5$ Pa is the surface pressure (Maykut 1982), and e is the saturation vapour pressure, calculated as $e = 611 \times 10^{7.5(T_0-273.16)/(T_0-35.86)}$ (Murray 1967).

At the polynya surface, the albedo α, the long-wave emissivity ε, the transfer coefficients C_{s} and C_{e} and the freezing point T_0 are set to 0.1, 0.99, 3×10^{-3}, 3×10^{-3} and 271.2 K, respectively, following Maykut (1982). The daily incident short-wave radiation, incoming long-wave radiation, air temperature and humidity were extracted from the NCEP reanalysis data.

The average heat fluxes across all polynya and lead water surface areas throughout the study region are presented in table 2 for the years 2003–2008. The net heat fluxes during January–March are negative, which means that the ocean releases heat to the atmosphere. Furthermore, solar radiation is quite weak during January–March, allowing the sensible heat flux to be 2–3 times that of latent flux or net long-wave radiation (and the net heat flux is therefore dominated by the sensible heat flux). In April, because of increasing solar radiation with concurrent decreasing sensible heat fluxes and net long-wave radiation (caused by increasing air temperatures), the net heat released by the ocean surface is significantly reduced. Furthermore, it is possible that ocean surfaces as a whole throughout the region obtain heat from the atmosphere during April of some years. The April time period can thus show extreme variability in net heat fluxes. When comparing average net heat fluxes during January–April across years, the average net heat fluxes in 2005 and 2007 are found to be relatively larger

than other years (i.e. less heat is lost from the ocean to the atmosphere in 2005 and 2007). Table 2 implies that this can possibly be attributed to larger sensible heat fluxes in January–February during these years owing to higher overall air temperatures.

Daily water areas (January–April from 2003 to 2008) and net heat loss from water surfaces of all polynyas in the study region are shown in figure 8. Open water areas play varying roles in the ocean–atmosphere heat balance depending on the time of year.

Table 2. Average atmosphere-ocean heat fluxes (MJ m^{-2} $month^{-1}$) for all polynya areas.

Month	Year	2003	2004	2005	2006	2007	2008
Jan	Net solar radiation	1.23	1.31	0.99	1.54	1.40	1.23
	Net long-wave radiation	−7.29	−7.77	−6.33	−10.21	−5.90	−8.86
	Sensible heat flux	−18.79	−25.98	−16.08	−39.89	−18.78	−32.77
	Latent heat flux	−7.35	−10.26	−6.84	−12.82	−5.67	−10.03
	Net heat flux	**−32.20**	**−42.71**	**−28.26**	**−61.38**	**−28.95**	**−50.44**
Feb	Net solar radiation	4.29	4.19	4.42	4.15	3.36	5.52
	Net long-wave radiation	−7.73	−6.68	−6.21	−5.47	−6.21	−9.24
	Sensible heat flux	−31.50	−25.42	−20.72	−9.63	−9.69	−31.42
	Latent heat flux	−11.10	−8.82	−7.54	−3.81	−3.95	−10.31
	Net heat flux	**−46.03**	**−36.72**	**−30.06**	**−14.77**	**−16.49**	**−45.45**
Mar	Net solar radiation	9.52	9.42	10.08	10.33	11.93	10.83
	Net long-wave radiation	−7.50	−6.41	−7.11	−6.36	−9.07	−8.66
	Sensible heat flux	−14.51	−12.03	−16.68	−13.95	−24.72	−26.20
	Latent heat flux	−6.47	−4.73	−6.72	−5.99	−9.14	−9.24
	Net heat flux	**−18.95**	**−13.75**	**−20.42**	**−15.97**	**−30.99**	**−33.27**
Apr	Net solar radiation	15.29	15.30	17.73	18.33	16.94	15.92
	Net long-wave radiation	−5.27	−5.54	−6.37	−7.97	−6.56	−6.00
	Sensible heat flux	−3.87	−6.30	−9.16	−17.56	−9.98	−7.27
	Latent heat flux	−2.25	−3.41	−4.66	−9.07	−4.98	−3.78
	Net heat flux	**3.90**	**0.04**	**−2.46**	**−16.27**	**−4.58**	**−1.14**
Avg	Net heat flux (Jan–Apr)	−23.32	−23.29	−20.30	−27.09	−20.25	−32.57

Note: Bold values indicate the average net atmosphere–ocean heat flux exchange for all polynya areas in the Bering Sea for each month and year of this study.

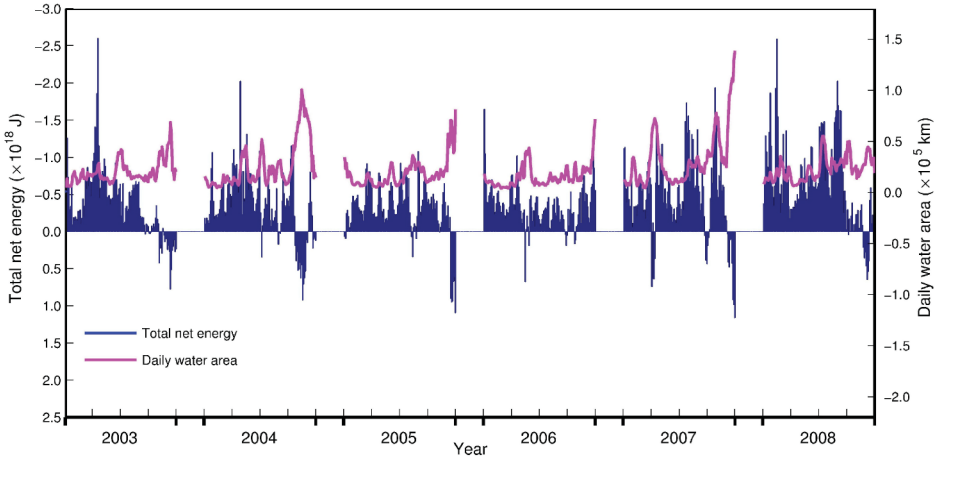

Figure 8. Comparison of daily water area (pink line) and net heat loss (blue line) from the atmosphere–ocean interface for all polynya regions in this study.

During January–March, increasing open water areas lead to more heat loss from the ocean surface to the atmosphere. But in April, owing to enhanced springtime incoming solar radiation, increasing water areas typically cause increased short-wave heat absorption and therefore heat gained by the ocean exceeds the heat lost from the ocean surface. These results indicate that the heat flux at the ocean surface cannot be determined directly from polynya areas, but rather must be interpreted in the context of the season and time of year as well. However, *a priori* knowledge of the net water area of polynyas and leads is critical and is the most important physical factor for accurate calculations of the heat flux through the surface of polynyas.

The results calculated here only include heat fluxes through water areas within the areal extent of polynyas. Although heat fluxes through thin ice cover can be important, we did not calculate heat fluxes through sea ice surfaces in this study. For heat fluxes through sea ice to be calculated, ice thickness data (in addition to ice concentration data) are critical. Until now, no ice thickness product has been issued for first-year ice regions, particularly for the small-scale thin ice regions inside polynyas in the Bering Sea region. Therefore, although total heat fluxes may be slightly underestimated here (owing to the inability to calculate heat fluxes through thin sea ice surfaces), our flux estimates are greatly improved compared to previous estimates because of our improved methodology to calculate accurate polynya net water areas.

3.4 *Major polynyas*

The Anadyr Gulf, St Lawrence Island and Cape Romanzo polynyas are investigated through the water areas in boxes A, B and C (figure 1). Table 3 shows the average values of daily water areas during January–March in the three polynya regions for 2003–2008. There is significant interannual variability in the area of polynyas in all the three regions. The average polynya water area for region A is significantly larger in 2007 and 2008 compared to the earlier years. This result corresponds to the extreme sea ice declines in these years for the summer Arctic Ocean and hints that the ice rapid retreat in 2007 summer may have initiated from the winter Anadyr Gulf. In contrast, however, the areas in regions B and C do not correspond to the Arctic sea ice minima of 2007 and 2008. Polynya areas in regions B and C are relatively small in these years, indicating a nearly opposite response with region A to the same regional wind field. With the exception of these regional inconsistencies during 2007 and 2008, the polynya areas of the three regions in the remaining years varied similarly. For instance, polynya areas in the three regions were all relatively large in 2003 and 2004 and small in 2006. In addition, we conclude that the sharply increasing total water area of all polynyas in the Bering Sea in 2007 (as described

Table 3. Average daily water areas ($\times 10^3$ km^2) during January–March for the A, B and C polynya regions.

Year	2003	2004	2005	2006	2007	2008
Box A	1.800	1.933	1.496	1.156	3.081	3.611
Box B	2.186	2.000	2.310	1.327	2.014	1.667
Box C	2.289	2.137	1.589	1.361	1.984	0.659

Notes: See figure 1 for regions. A, Anadyr Gulf polynya; B, St Lawrence Island polynya; C, Cape Romanzo polynya.

in §3.2) is mainly attributable to the dramatic expansion of the region A polynyas, which is the largest and arguably the most critical polynya system in the northern Bering Sea.

The general coastline orientations of the three polynya regions A, B and C are shown in boxes A, B and C (figure 1, dashed line). Daily mean offshore winds in regions A, B and C are calculated based on the daily winds from the NCEP reanalysis data. A running correlation coefficient R_i between wind speed and polynya water area can be used to investigate potential driving mechanisms for polynya development, as used by Zhao *et al.* (2006). It is defined as

$$R_i = \frac{\sum_{k=i-n}^{i+n} \left(X_k - \overline{X}_k\right)\left(Y_k - \overline{Y}_k\right)}{\sqrt{\sum_{k=i-n}^{i+n} \left(X_k - \overline{X}_k\right)^2} \sqrt{\sum_{k=i-n}^{i+n} \left(Y_k - \overline{Y}_k\right)^2}}, \; i = 1+n, \ldots, N-n, \tag{4}$$

where X_k is the daily water area of the kth day; $\overline{X}_k$ is the mean of X_k; Y_k is the daily mean offshore wind of the kth day; $\overline{Y}_k$ is the mean of Y_k; n is the window width of running correlation; and N is the number of samples. The running correlation coefficient R_i shows the degree that daily water area is related to daily mean offshore wind on a timescale of n days. Here, n is set to 15 days.

Figure 9 indicates that the correlation between polynya water area and offshore wind speeds varies among the three polynya regions. The positive correlation between water areas and offshore wind speeds in polynya region C is the strongest, whereas that for the polynya region A is noticeably weaker. In the polynya region B, both the offshore and shoreward winds can promote the opening of water areas. Both the eastern and northern portions of the polynya region C are land, which is very prone to form latent heat polynyas. In addition, the northward flowing, warm Anadyr Current in polynya region A also may influence the size of the polynyas in region A. This may explain why the running correlation coefficients in polynya region A are generally lower than those in polynya region C. Not only offshore winds may cause polynya formation along the southern coastlines of St Lawrence Island, but shoreward winds may also cause polynyas to form along the northern coastlines. Therefore, water areas may correlate either negatively or positively with offshore winds in polynya region B. In addition, winds may not only intensify the divergence of ice and promote water area growth in a polynya, but can also enhance the turbulent exchange across the surface waters of the polynya. The larger the turbulent exchange, the more the heat will be lost to the atmosphere, which accelerates the freezing rate and inhibits the growth of water areas within polynyas. For example, Pease (1987) suggested that increasing wind speeds above 5 m s^{-1} did not increase the maximum size a polynya could achieve, but could increase the rate at which the maximum size was attained. As a result, offshore wind speeds may not always positively impact the overall size of a polynya (see figure 9).

The erosion algorithm based on greyscale morphology methods can be used for any spatial resolution data. To compare our results using the 12.5 km resolution sea ice product with the higher spatial resolution 6.25 km product, we compared results based on sea ice concentrations for 1 March 2003, which is provided by Spreen *et al*. (2008). The pack ice edge of the 6.25 km resolution image obtained by the erosion algorithm is compared with that of our 12.5 km resolution (figure 10). The total water area and

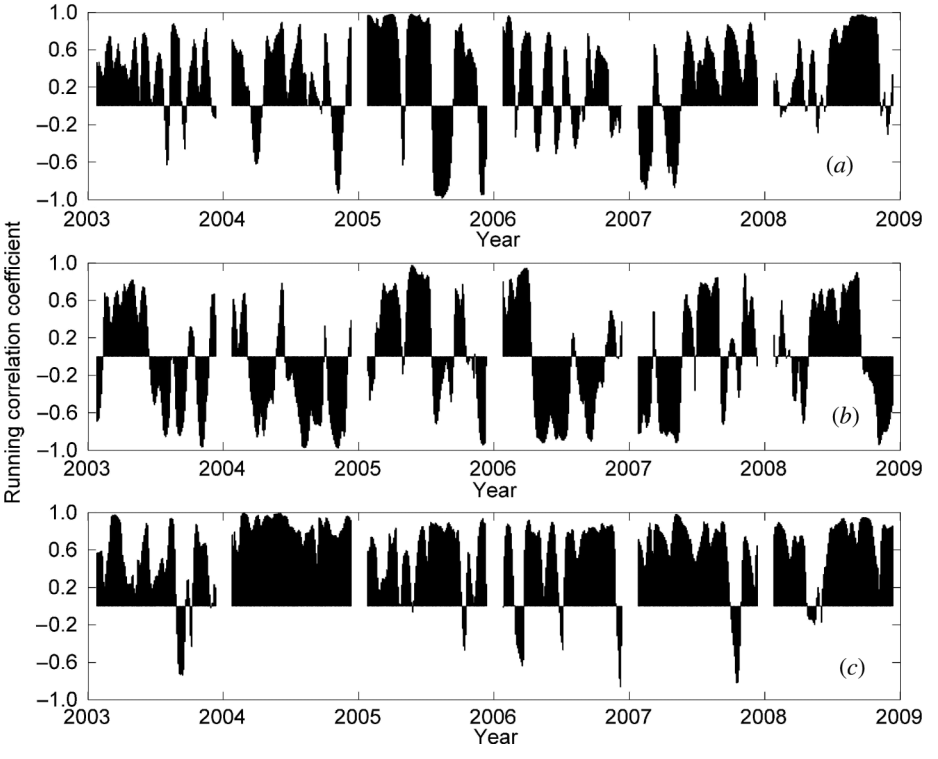

Figure 9. Daily time series of correlation coefficients between the water areas and average offshore winds for the region A, B and C shown in (*a*), (*b*) and (*c*), respectively.

the mean heat loss within all polynyas or leads obtained by the 6.25 km resolution data are 40 953 km^2 and 224.1 W m^{-2}, respectively, while those obtained by the 12.5 km resolution data are 38 180 km^2 and 193.1 W m^{-2}, respectively. Although spatial resolution may cause some minimal discrepancies between these calculated results,

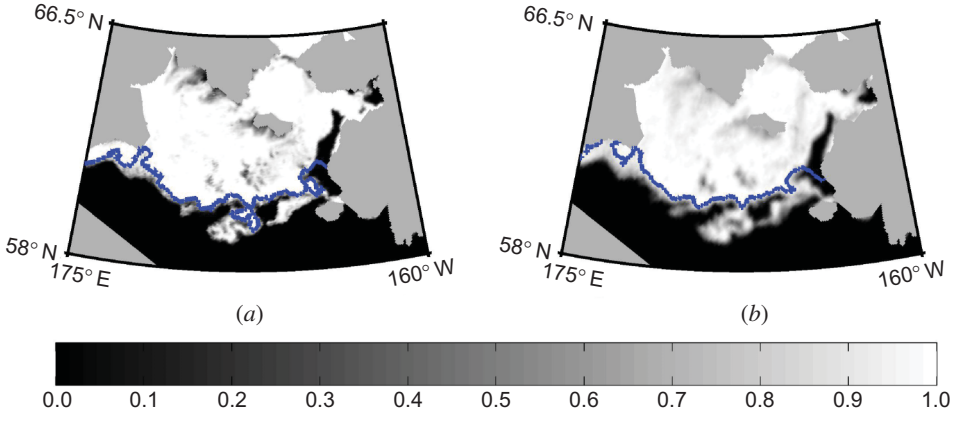

Figure 10. Daily sea ice concentrations showing the pack ice edge (blue line) for 1 March 2003. (*a*) 6.25 km resolution AMSR-E sea ice concentration data and (*b*) 12.5 km resolution AMSR-E sea ice concentration data.
Note: AMSR-E, Advanced Microwave Scanning Radiometer-EOS.

the similarities between both water area and heat loss values for these two resolution data sets support the overall robustness of our erosion algorithm (and applicability at multiple spatial scales).

5. Summary and conclusions

The erosion algorithm based on greyscale morphology image-processing techniques applied to satellite-derived sea ice concentrations is shown to be a tractable method of obtaining the extent of pack ice within the northern Bering Sea. The area of polynyas can subsequently be derived using the water integration method within the extent of the pack ice. Using these techniques, water areas of all polynyas in the Bering Sea (January–April of 2003–2008) are obtained from daily AMSR-E sea ice concentrations. Compared with those areas calculated with more traditional sea ice concentration threshold methods (in this case at 0.75), the integrated water areas derived using greyscale morphology are more accurate representations of water areas in all polynyas (i.e. the actual net water area) and additionally eliminate the need for artificially removing the marginal ice zone (as is the case with the more traditional threshold methods). Moreover, erosion techniques provide accurate and more reliable polynya and/or lead water areas by avoiding potential inaccurate calculations arising from the choice of an arbitrary sea ice concentration threshold.

Investigation of the interseasonal variability of monthly water areas suggests that those during January are relatively small compared with that of other months for most years. Monthly water areas during February and March are somewhat larger, whereas those during April are the largest. During January, much of the Bering Sea is not yet ice covered, which could explain why polynya areas are relatively small during this month. However, during April, the solar flux positive feedback from such large polynya areas is one of the most important factors that promote even larger water areas during this month. Furthermore, it is found that the total polynya water area in 2007 is largest compared to the other years, which is also consistent with the lowest record of summer sea ice extent for the Arctic as a whole.

According to the calculated heat fluxes across the atmosphere–ocean interface, we conclude that the ocean releases heat to the atmosphere for all polynya areas during January–March. Heat lost in the form of sensible heat exchange is largest, which is 2–3 times larger than the latent heat exchange or long-wave radiation. In April, because of the accumulation of solar radiation and warming air temperatures, the heat lost by the ocean surface is nearly 0 (and can even gain heat from the atmosphere in some years). Therefore, increasing polynya water areas during January–March can cause the ocean to be a heat source to the atmosphere, while increasing polynya water areas during April can cause that the ocean to be a heat sink from the atmosphere.

Polynya water areas and their correlation with offshore winds in the Anadyr Gulf, St Lawrence Island and Cape Romanzo polynyas are also investigated. Water areas in the St Lawrence Island and Cape Romanzo polynyas have exhibited significant interannual variability in size over time. In particular, the interannual variability within the Anadyr Gulf polynya region increased sharply in 2007. In addition, the interannual variability of water areas in the Anadyr Gulf polynya is nearly the same as the variability of the total water area within the entire Bering Sea. We can therefore conclude that the Anadyr Gulf polynya is the largest and most active polynya in the Bering Sea. Correlation coefficients between the polynya water areas and offshore winds are highest for the Cape Romanzo polynya. In addition to offshore winds, shoreward winds

can also induce the formation of the polynya (e.g. along the north coast of St Lawrence Island). Because the warm, northwards moving Anadyr Current also may influence polynya activity, the correlation between the size of the Anadyr Gulf polynya and offshore winds is weaker within this region.

Acknowledgement

This research was supported by Global Change Research Programme of China (Grant # 2010CB951403 and 2008AA121701) and the US National Science Foundation Arctic Natural Sciences Program (Grant # 0713939).

References

Aagaard, K., Coachman, L.K. and Carmack, E.C., 1981, On the halocline of the Arctic Ocean. *Deep-Sea Research*, **28**, pp. 529–545.

Cavalieri, D.J. and Martin, S., 1994, The contribution of Alaskan, Siberian, and Canadian coastal polynyas to the cold halocline layer of the Arctic Ocean. *Journal of Geophysical Research*, **99**, pp. 18343–18362.

Comiso, J.C. and Gordon, A.L., 1998, Interannual variability in summer sea ice minimum, coastal polynyas and bottom water formation in the Weddell Sea. In *Antarctic Sea Ice: Physical Processes, Interactions and Variability, Antarctic Research Series*, Vol. 74, M.O. Jeffries (Ed.), pp. 293–315 (Washington, DC: AGU).

Comiso, J.C., Parkinson, C.L., Gersten, R. and Stock, L., 2008, Accelerated decline in the Arctic sea ice cover. *Geophysical Research Letters*, **35**, pp. 1–6.

Dougherty, E.R. (Ed.), 1993, *Mathematical Morphological Image Processing*, p. 255 (New York: Marcel Dekker).

Emms, P.W., 1997, Streamtube models of gravity currents in the ocean. *Deep-Sea Research Part I*, **44**, pp. 1575–1610.

Grebmeier, J.M. and Cooper, L.W., 1995, Influence of the St. Lawrence Island polynya upon the Bering Sea benthos. *Journal of Geophysical Research – Oceans*, **100**, pp. 4441–4460.

Grumbine, R.W., 1991, A model of the formation of high-salinity shelf water on polar continental shelves. *Journal of Geophysical Research – Oceans*, **96**, pp. 22049–22062.

Haltiner, G.J. and Martin, F.L. (Eds.), 1957, *Dynamical and Physical Meteorology*, p. 470 (New York: McGraw-Hill).

Hess, S.L. (Ed.), 1959, *Introduction to Theoretical Meteorology*, p. 362 (New York: Holt, Rinehart and Winston).

Kern, S., Spreen, G., Kaleschke, L., Rosa, S.D.L. and Heygster, G., 2007, Polynya signature simulation method polynya area in comparison to AMSR-E 89 GHz sea-ice concentrations in the Ross Sea and off the Adelie Coast, Antarctica, for 2002–05: first results. *Annals of Glaciology*, **46**, pp. 409–418.

Kwok, R., Comiso, J.C., Martin, S. and Drucker, R., 2007, Ross Sea polynyas: response of ice concentration retrievals to large areas of thin ice. *Journal of Geophysical Research*, **112**, C12012, doi:10.1029/2006JC003967.

Maqueda, M.A.M., Willmott, A.J. and Biggs, N.R.T., 2004, Polynya dynamics: a review of observations and modeling. *Reviews of Geophysics*, **42**, RG1004, doi:10.1029/2002RG000116.

Markus, T. and Burns, B.A., 1995, A method to estimate subpixel-scale coastal polynyas with satellite passive microwave data. *Journal of Geophysical Research – Oceans*, **100**, pp. 4473–4487.

Massom, R.A., Harris, P.T., Michael, K.J. and Potter, M.J., 1998, The distribution and formative processes of latent-heat polynyas in East Antarctica. *Annals of Glaciology*, **27**, pp. 420–426.

Maykut, G.A., 1982, Large-scale heat exchange and ice production in the central Arctic. *Journal of Geophysical Research – Oceans*, **87**, pp. 7971–7984.

MAYKUT, G.A. and MCPHEE, M.G., 1995, Solar heating of the Arctic mixed layer. *Journal of Geophysical Research – Oceans*, **100**, pp. 24691–24703.

MAYKUT, G.A. and PEROVICH, D.K., 1987, The role of shortwave radiation in the summer decay of a sea ice cover. *Journal of Geophysical Research*, **92**, pp. 7032–7044.

MCNUTT, L., 1981, Remote sensing analysis of ice growth and distribution in the eastern Bering Sea. In *The Eastern Bering Sea Shelf Oceanography and Resources*, D.W. Hood and J.A. Calder (Eds.), Vol. 1, pp. 141–165 (Washington, DC: US National Oceanographic and Atmospheric Administration).

MURRAY, F.W., 1967, On the computation of saturation vapor pressure. *Journal of Applied Meteorology*, **6**, pp. 203–204.

NIEBAUER, H.J., BOND, N.A., YAKUNIN, L.P. and PLOTNIKOV, V.V., 1999, An update on the climatology and sea ice of the Bering Sea. In *Dynamics of the Bering Sea*, T.R. Loughlin and K. Ohtani (Eds.), pp. 33–34 (Fairbanks, AK: University of Alaska Sea Grant).

PARMIGGIANI, F., 2006, Fluctuations of Terra Nova Bay polynya as observed by active (ASAR) and passive (AMSR-E) microwave radiometers. *International Journal of Remote Sensing*, **27**, pp. 2459–2467.

PEASE, C.H., 1987, The size of wind-driven coastal polynyas. *Journal of Geophysical Research*, **92**, pp. 7049–7059.

SMEDSRUD, L.H., BUDFELL, W.P., JENKINS, A.D. and ADLANDSVIK, B., 2006, Fine-scale sea-ice modelling of the Storfjorden polynya, Svalbard. *Annals of Glaciology*, **44**, pp. 1–7.

SMITH, S.D., MUENCH, R.D. and PEASE, C.H., 1990, Polynyas and leads: an overview of physical processes and environment. *Journal of Geophysical Research*, **95**, pp. 9461–9479.

SPREEN, G., KALESCHKE, L. and HEYGSTER, G., 2008, Sea ice remote sensing using AMSR-E 89-GHz channels. *Journal of Geophysical Research*, **113**, C02S03, doi:10.1029/2005JC003384.

STIRLING, I., 1997, The importance of polynyas, ice edges, and leads to marine mammals and birds. *Journal of Marine Systems*, **10**, pp. 9–21.

STRINGER, W.J. and GROVES, J.E., 1991, Location and areal extent of polynyas in the Bering and Chukchi Seas. *Arctic*, **44**, pp. 164–171.

WINSOR, P. and BJORK, G., 2000, Polynya activity in the Arctic Ocean from 1958 to 1997. *Journal of Geophysical Research*, **105**, pp. 8789–8803

WORLD METEOROLOGICAL ORGANIZATION (WMO), 1970, *WMO Sea Ice Nomenclature*, WMO Report No. 259, TP 145, 147 p. + 8 supplement (Geneva: WMO).

ZHAO, J., CAO, Y. and SHI, J., 2006, Core region of Arctic Oscillation and the main atmospheric events impact on the Arctic. *Geophysical Research Letters*, **33**, L22708, doi:10.1029/2006GL027590.